Types of Papers

Research Papers

Title

Optical dissection of synaptic plasticity for early adaptation in *Caenorhabditis elegans*

Author names and affiliations

Keita Ashida[1] (12ashi.jkkt@keio.jp)
Hisashi Shidara[1] (hisa.shidara@sci.hokudai.ac.jp)
Kohji Hotta[1] (khotta@keio.jp)
Kotaro Oka[123*] (oka@bio.keio.ac.jp)

[1]Department of Biosciences and Informatics, Faculty of Science and Technology, Keio University, Yokohama 223-8522, Japan
[2]Graduate Institute of Medicine, College of Medicine, Kaohsiung Medical University, Kaohsiung City, 80708, Taiwan.
[3]Waseda Research Institute for Science and Engineering, Waseda University, 2-2 Wakamatsucho, Shinjuku, Tokyo 162-8480, Japan

Corresponding author

Kotaro Oka, Department of Biosciences and Informatics, Faculty of Science and Technology, Keio University, Yokohama 223-8522, Japan.
E-mail: oka@bio.keio.ac.jp
Phone number: +81-45-566-1700
Fax: +81-45-566-1789

Present/permanent address

Keita Ashida, Present address: Universal Biology Institute, Graduate School of Science, The University of Tokyo, 113-0033 Tokyo, Japan.
Hisashi Shidara, Present address: Department of Biological Sciences, Faculty of Science, Hokkaido University, Sapporo 060-0810, Japan.

Abstract

To understand neuronal information processing, it is essential to investigate the input–output relationship and its modulation via detailed dissections of synaptic transmission between pre- and postsynaptic neurons. In *Caenorhabditis elegans*, pre-exposure to an odorant for five minutes reduces chemotaxis (early adaptation). AWC sensory neurons and AIY interneurons are crucial for this adaptation; AWC neurons sense volatile odors, and AIY interneurons receive glutamatergic inputs from AWC neurons. However, modulations via early adaptation of the input–output relationship between AWC and AIY are not well characterized. Here we use a variety of fluorescent imaging techniques to show that reduced synaptic-vesicle release without Ca^{2+} modulation in AWC neurons suppresses the Ca^{2+} response in AIY neurons via early adaptation. First, early adaptation modulates the Ca^{2+} response in AIY but not AWC neurons. Adaptation in the Ca^{2+} signal measured in AIY neurons is caused by adaptation in glutamate release from AWC neurons. Further, we found that a G protein γ-subunit, GPC-1, is related to modulation of glutamate input to AIY. Our results dissect the modulation of the pre- and postsynaptic relationship *in vivo* based on optical methods, and demonstrate the

importance of neurotransmitter-release modulation in presynaptic neurons without Ca^{2+} modulation.

Keywords

Fluorescent imaging, chemosensation, olfaction, learning, neurotransmitter, synaptic plasticity

Highlights

- The input–output relationship is dissected by Ca^{2+}, glutamate and synaptic release imaging.
- An interneuron shows Ca^{2+} response modulation by adaptation, but not a sensory neuron.
- Synaptic release from the sensory neuron and glutamate inputs to the interneuron are modulated.
- G protein γ-subunit is related to the glutamate modulation.

Abbreviation

C. elegans, *Caenorhabditis elegans*;

C.I., chemotaxis index;

cGMP, cyclic guanosine monophosphate;

n.s., not significant;

N. A., numerical aperture;

NGM, nematode growth medium;

PKC, protein kinase C;

SEM, standard error of the mean;

SNARE, soluble N-ethylmaleimide-sensitive factor attachment protein receptor;

WT, wildtype

Introduction

Clarifying the input–output relationship and its modulation is fundamental for understanding neuronal information processing, and detailed dissection of the synaptic transmission between pre- and postsynaptic neurons is required. Electrophysiological and imaging techniques have revealed pre- and postsynaptic neuronal activity modulation (Friauf et al., 2015; Petzoldt et al., 2016; Nanou and Catterall, 2018). However, the relationship between pre- and postsynaptic neurons *in vivo* is still largely unknown due to the complexity of the networks involved (Ogawa and Oka, 2015; Prešern et al., 2015; Stuart and Spruston, 2015).

The nematode, *Caenorhabditis elegans* is suitable for such investigations, due to its simple neuronal network, the availability of detailed information regarding its neuronal connectivity (White et al., 1986; Cook et al., 2019), and its transparent body, which facilitates imaging (Kerr and Schafer, 2006). However, although previous imaging studies have visualized synaptic-vesicle release and neurotransmitter input (Marvin et al., 2013; Ventimiglia and Bargmann, 2017; Ashida et al., 2019), no research has directly reported modulations of both the pre- and postsynaptic relationships.

In *C. elegans*, pre-exposure to odor reduces chemotaxis to the odorant (Colbert and Bargmann, 1995; Hirotsu and Iino, 2005; Yamada et al., 2009). A specific type of adaptation, known as early adaptation, can be induced by five minutes of pre-exposure, and AWC sensory neurons and AIY interneurons play crucial roles in this process (Hirotsu and Iino, 2005; Yamada et al., 2009). AWC neurons sense volatile odors, and AIY interneurons receive inhibitory glutamatergic inputs from the AWC (Horoszok et al., 2001; Wenick and Hobert, 2004; Chalasani et al., 2007); decreasing of glutamate inputs by odor stimulation evokes Ca^{2+} response in AIY (Chalasani et al., 2007; Ashida et al., 2019). These neurons are also necessary for odor attraction (Bargmann et al., 1993; Gray et al., 2005; Yoshida et al., 2012). While the molecular basis of early adaptation has been investigated in depth (Hirotsu and Iino, 2005; Yamada et al., 2009), how neuronal activity is modulated in AWC and AIY neurons remain unknown. To understand such modulation, the neural activity of both AWC and AIY neurons, and the synaptic transmission between them must be investigated in detail.

Here, we used several fluorescent imaging techniques to characterize Ca^{2+} response modulations in AWC and AIY, synaptic-vesicle release in AWC neurons and glutamate inputs to AIY neurons following early adaptation. We show that early adaptation does not modulate the Ca^{2+} response to odor in AWC, but that it does suppress the Ca^{2+} response in AIY neurons. Moreover, both synaptic-vesicle release from AWC and glutamate inputs to AIY are also reduced corresponding to the Ca^{2+} modulations in AIY neurons. Finally, we show that a G protein γ-subunit, GPC-1, is related to both early adaptation and glutamate modulation. Our results reveal that modulations of the pre- and postsynaptic relationship *in vivo*, via imaging techniques and provide evidence of a new type of neurotransmitter release modulation without Ca^{2+} modulation *in vivo*.

Materials and Methods

Ethical approval

All animal work was approved by the Keio University Institutional Animal Care and Use Committee.

Molecular biology.

Gateway Destination vectors for expressing proteins and Gateway Entry vectors for cell-specific promoters (Thermo Fisher Scientific) were obtained from the Comprehensive Brain Science Network. All plasmids used to express proteins in the worms were generated from these vectors using Gateway Cloning Technology (Thermo Fisher Scientific).

C. elegans strains and culture conditions.

The nematodes were cultured at 20 ºC on nematode growth medium (NGM) agar plates with *Escherichia coli* OP50 bacteria under standard conditions (Brenner, 1974). The

wild-type animals were Bristol strain N2, and hermaphrodites were used for all experiments. Transgenic animals were created by microinjecting plasmids into N2 and JN372 *gpc-1* (pe372) X strains. The transgenic strains used for the present study were as follows: *okaEx4[pstr-2::GEM-GECO1, 100 ng/μL]*, *okaEx10[pttx-3::G-CaMP6, 50 ng/μL + pttx-3::dimer2, 50 ng/μL]*, *okaEx11[pttx-3::iGluSnFR, 75 ng/μL]*, and *okaEx12; gpc-1(pe372) X [pttx-3::iGluSnFR, 75 ng/μL]*. The strain expressing VGLUT-pHluorin was CX16644 (kyIs623: UV-integrated kyEx4435 AWCON VGLUT-pH Line. Backcrossed to N2 11x) (Ventimiglia and Bargmann, 2017).

Ca^{2+}, glutamate and VGLUT-pHluorin imaging

We used a genetically encoded Ca^{2+} indicator, GEM-GECO1 (Zhao et al., 2011), for Ca^{2+} imaging, a genetically encoded glutamate indicator, iGluSnFR (Marvin et al., 2013), for glutamate imaging, and VGLUT-pHluorin (Ventimiglia and Bargmann, 2017) for synaptic-vesicle release imaging using olfactory chips (Chronis et al., 2007). For Fig. 2, we used a Ca^{2+} indicator, G-CaMP6 (Ohkura et al., 2012), and dimer2 (RFP as reference). The olfactory chips are micro fluidic devices that can control odor

stimulation temporally via valve switching. The worms were exposed to S-basal buffer or isoamyl alcohol (IAA) diluted with S-basal buffer (10^{-4} concentration) for a total duration of 4 min and 40 s before imaging commenced. After pre-exposure, animals were stimulated sequentially as follows: (1) 20 s in diluted IAA (first stimulation); (2) 1 min 40 s in S-basal buffer; (3) 20 s in diluted IAA (second stimulation); and (4) 40 s in S-basal buffer (see Fig. 1A). For Fig. 2, we only recorded the response to the second stimulation, but we recorded for an additional 20 s after the second stimulation (Fig. 2A) because AIY interneurons only show the Ca^{2+} responses to odor addition clearly (Chalasani et al., 2007). In Fig. 4, only the response to the second stimulation was recorded for avoiding photobleaching (Fig. 4A) because background autofluorescence shows significant photobleaching during pHluorin imaging (Ventimiglia and Bargmann, 2017). We used an inverted microscope (IX71, Olympus) with an LED light source (SOLA, Lumencor), and a 3CCD camera (C7800-20, Hamamatsu Photonics). Images were acquired every 100 ms (the exposure time was also 100 ms) on an AQUACOSMOS (Hamamatsu Photonics) for all experiments. For Ca^{2+} and glutamate imaging, a 20× objective lens (UCPLFLN 20X, N. A.: 0.7, Olympus) and a 1.6× zoom

lens were used. For pHluorin imaging, a 60× oil-immersion lens (UPLSAPO 60XO, N. A.: 1.35, Olympus) was used. U-MWBV2 (Olympus) fluorescent filter cubes were used for Ca^{2+} imaging (GEM-GECO), BrightLine GFP/DSRED-A (semrock) cubes were used for Ca^{2+} imaging (G-CaMP6 and dimer2), and U-MWIB3 (Olympus) cubes were used for glutamate and pHluorin imaging, respectively. To reduce noise caused by movement of the worms', S-basal buffer containing a cholinergic agonist, levamisole (2 mM), was used for glutamate and pHluorin imaging. We also noted that we imaged pHluorin a little brightly rather than avoided photobleaching to detect the decrease in the fluorescent intensity by odor application because the sensor is not so bright (see Fig. 4).

Chemotaxis assays

Chemotaxis assays were performed based on previous research (Hirotsu and Iino, 2005). Briefly, the cultivated worms were collected in a microtube and washed three times with S-basal buffer. Animals were pre-exposed to S-basal buffer with (exposed) or without (mock) IAA at a concentration of 10^{-4} for 5 min. Next, 500 mM of sodium

azide (1 μL) was spotted on two points on both sides of an assay plate. After pre-exposure, the animals were washed three times with S-basal buffer and spotted on the center of an assay plate. IAA was diluted (10^{-2}) in ethanol and spotted on one side of the plate (1 μL); ethanol was spotted on the other side as a control (1 μL). These spotting sites were the same as those used for the sodium azide solution. Animals were spotted at the center of the plate, and excess medium was immediately removed using a tissue. Animals were counted 30 min after they had been spotted on the plate. The chemotaxis index was calculated as (A − B) / (A + B), with A being the number of animals on the odorant-spotted side and B being the number of animals on the ethanol-spotted side (the counting area was the same as that used in Hirotsu et al., 2009). In the control experiments, worms were spotted on the plates just after collection and washed three times.

Data analysis and statistical tests

We analyzed the imaging data using the semi-automated custom software written in MATLAB (MathWorks) that was used in a previous study (Shidara et al., 2017).

Regions of interests were determined based on the morphology of the neurons. For AIY neurons, we measured the Ca^{2+} response and glutamate inputs at the neurite, because these interneurons show a Ca^{2+} response clearly at the neurite, but not at the soma (Clark et al., 2006; Chalasani et al., 2007). The fluorescent intensity data ($\Delta F/F$ or $\Delta R/R$) in Figs. 2B, 3B, C, and 5B, C were normalized by the average intensities during the first 2 s. The data in Fig. 1 were normalized by the average intensities during the 2 s just before removal of the second odor, because odor addition immediately decreased Ca^{2+} levels. The data in Fig. 4B were normalized by the average intensities during 2 s just before odor addition, to reduce the effect of photobleaching.

Statistical tests were performed in R (R Project), Welch's t-test and paired sample t-test were performed using the t.test function, the test for the Pearson product-moment correlation coefficient was performed using the cor.test function, Dunnett's test was performed using the glht function in the multcomp library, and the power analysis for the t-test was performed using the t.test function in pwr library.

The Ca^{2+} response intensities shown in the box plots (first and second in Fig. 1B, C) were calculated by subtracting the averaged intensity over the 20 s before odor

removal from the maximal intensity during the 20 s period after removal. The decrease intensities (decrease in Fig. 1B, C) were calculated by subtracting the averaged intensity over the 20 s before second odor addition from the minimal intensity during the 20 s period after addition. To determine the sample size, we performed a power analysis using value of the first and second responses for the soma of pre-exposed animals. The resultant sample size, give a power of over 0.8 with Glass's Δ.

The Ca^{2+} response intensity shown in Fig. 2B was calculated by subtracting the averaged intensity over the 20 s before odor application from the maximal intensity during the 20 s period after odor application.

The glutamate-input intensities (first and second in Fig. 3C) were produced by subtracting the averaged intensity for the 20 s before odor removal from the maximal intensity during the 20 s period after removal. Decreasing intensities (decrease in Fig. 3C) were calculated by subtracting the minimal intensity during the 20 s period after the second odor addition from the averaged intensity during the 20 s period before addition. The fluorescence intensities shown in Fig. 3D were normalized using the averaged

intensity for the 2 s period 80 s after imaging onset. Then, the averaged intensity for the 20 s period before (pre-odor) and during (during odor) odor stimulation was calculated.

The levels of decrease shown in Fig. 4C (left) were calculated as $-1 \times$ the minimal value occurring from 20−40 s in Fig. 4B, because intensities were normalized to zero at 20 s. For Fig. 4C (right), intensities (ΔF/F) were normalized using the average intensity for the 2 s just before odor removal. After the normalization, increased levels were determined as the maximal values for the 40−60 s period.

The chemotaxis indices shown in Fig. 5A were calculated as described above. To determine the sample size, we performed a power analysis using the control and exposed values for wild-type animals. The power for the resulting the sample size is over 0.8, using Glass's Δ. In preparing Fig. 5C, D, we used the same procedure as described for Fig. 3. To determine the sample size, we performed a power analysis using the response intensities for the first simulation in the control and pre-exposed wild-type animals. The power for the resulting sample size is over 0.8 with Glass's Δ.

Results

AIY but not AWC neurons exhibit modulation of Ca^{2+} response modulation by early adaptation

To identify AWC and AIY modulations by early adaptation, we measured the Ca^{2+} response of both neurons with (exposed) and without (control) 5 min of IAA pre-exposure (Fig. 1A). Here, we assumed that modulation by early adaptation would be observed in the responses following pre-exposure (the second stimulation in Fig. 1A). In addition, to examine the response to pre-exposure, we assessed the first response.

First, we measured Ca^{2+} responses in AWC neurons. AWC neurons showed an off-response and a larger Ca^{2+} response amplitude at the soma after 5 min of stimulation than after 20 s of stimulation (the first stimulation in Fig. 1B) as observed in previous research (Chalasani et al., 2007). Conversely, the response in AWC neurons to the second stimulation did not change significantly following pre-exposure (Fig. 1B, second stimulation). Because axonal Ca^{2+} is more crucial for synaptic transmission than somatic Ca^{2+} (Shidara et al., 2013; Hawk et al., 2018), we also investigated the axonal Ca^{2+} response in AWC neurons. The Ca^{2+} response to both the first and second

stimulation was not modulated at the axon (Fig. 1C). These results indicate that the Ca^{2+} response in AWC neurons is not modulated by early adaptation.

Next, we investigated the Ca^{2+} response in the AIY with and without odor pre-exposure (Fig. 2). Ca^{2+} responses in AIY were observed even without odor stimulation, but often following odor application (Fig. 2A) as previous research (Chalasani et al., 2007). In contrast to the AWC neurons, the response in AIY neurons decreased significantly (Fig. 2B). Thus, the Ca^{2+} response to odor is reduced by early adaptation in AIY interneurons but not in AWC neurons.

Glutamate input to AIY neurons is modulated by early adaptation

The Ca^{2+} response was modulated in AIY but not in AWC neurons by early adaptation. Despite these findings, neurotransmission from AWC could still affect the Ca^{2+} response in AIY neurons. AWC neurons release glutamate to AIY, and the AIY interneurons receive inhibitory inputs via a glutamate-gated chloride channel (Horoszok et al., 2001; Wenick and Hobert, 2004; Chalasani et al., 2007; Serrano-Saiz et al., 2013). This suggests that glutamate input probably regulates neural activity in AIY

neurons. Recently, we identified that the decrease of glutamate inputs to AIY evokes Ca^{2+} response in AIY (Ashida et al., 2019). We, therefore, evaluated glutamate inputs to AIY neurons using a fluorescent glutamate indicator, iGluSnFR (Marvin et al., 2013), which was expressed on the outside of the AIY cell membrane during early adaptation.

Glutamate inputs to AIY neurons decreased following odor application and increased transiently following odor removal (Fig. 3B) as we previously reported (Ashida et al., 2019). These glutamate increases and decrease is consistent with the Ca^{2+} response to odor in AWC neurons (Fig. 1), indicating that changes in glutamate input is related to AWC activity. Odor pre-exposure suppressed the increase in glutamate input following odor removal (20-40 s, and 140–160 s in Fig. 3B) and the decreases following odor addition (120–140 s in Fig. 3B; Fig. 3C). Moreover, odor application significantly decreased glutamate inputs in control animals (comparing with 100–120 s and 120–140 s in Fig. 3B, see Materials and Methods), but this decline following odor application was abolished by pre-exposure (Fig. 3D). Therefore, we conclude that the glutamate input response to AIY is inhibited by early adaptation.

Synaptic-vesicle release in AWC neurons is modulated by early adaptation

Thus, glutamate input to AIY interneurons was modulated by odor pre-exposure. However, AIY neurons receive glutamate from various neurons (White et al., 1986; Serrano-Saiz et al., 2013; Cook et al., 2019), so whether the glutamate modulation we observed originated with AWC neurons was still unknown. To address this question, we measured synaptic-vesicle release in AWC neurons.

To visualize this process, we used VGLUT-pHluorin (Ventimiglia and Bargmann, 2017), which is a pH-sensitive variant of GFP that can detect pH differences between the inside and outside of synaptic vesicles (Miesenböck et al., 1998). Compared with Ca^{2+} and glutamate imaging, VGLUT-pHluorin imaging is more sensitive to photo-bleaching, so we only examined the second stimulus (Fig. 4A).

Synaptic-vesicle release was reduced by odor addition and increased by odor removal in the same manner as the Ca^{2+} response in AWC neurons (Fig. 4B), which is consistent with previous research (Ventimiglia and Bargmann, 2017). Pre-exposure suppressed increases in synaptic-vesicle release following odor removal and decreases following odor application (Fig. 4C). These results are consistent with the pattern

observed in glutamate input to AIY. Combined, these results show that the AWC neurons' synaptic-vesicle release in response to odor is modulated by early adaptation, despite the fact that the Ca^{2+} response is not.

The G protein γ-subunit, GPC-1, is related to modulation by early adaptation

While synaptic-vesicle release modulation was demonstrated, the mechanism responsible for the modulation remained unknown. In previous research, the G protein γ-subunit, GPC-1, has been shown to play a crucial role in AWC neurons, and *gpc-1* mutants are defective in early adaptation to a specific odorant, benzaldehyde, at a behavioral level (Yamada et al., 2009). Thus, we first investigated whether *gpc-1* mutants also exhibit defects in early adaptation to IAA at the behavioral level (Fig. 5A). These mutants were defective in their adaptation to IAA, indicating that GPC-1 could also play a crucial role in early adaptation to IAA.

We then evaluated glutamate release in *gpc-1* mutants. Glutamate inputs to AIY neurons increased following odor removal and decreased following odor application, as found for wild types (Figs. 3, 5B). However, these declines and increases

were not suppressed by odor pre-exposure (Fig. 5C, D), indicating that *gpc-1* mutants have defective glutamate modulation. Based on these findings, we conclude that the G protein γ-subunit, GPC-1, is related to glutamate modulation by early adaptation.

Discussion

We used imaging techniques to investigate modulations of the relationship between AWC and AIY neurons that occur as a result of early adaptation and showed that synaptic-vesicle release in AWC neurons is reduced without any change in the Ca^{2+} response. Ca^{2+} imaging of AWC and AIY neurons indicates that the AWC Ca^{2+} response remains unchanged after early adaptation, but that the Ca^{2+} response in AIY decreases after 5 min of odor pre-exposure (Figs. 1,2). We also found that the response of glutamate input to AIY neurons is suppressed by pre-exposure (Fig. 3). The VGLUT-pHluorin imaging in AWC neurons showed that the response of synaptic-vesicle release is also inhibited by pre-exposure (Fig. 4). The G protein γ-subunit, GPC-1, is required for both glutamate modulation and early adaptation (Fig. 5). These results are the first to demonstrate AWC synaptic-vesicle release modulation without Ca^{2+} modulation as a result of early adaptation.

In previous studies (Euler et al., 2002; Frick et al., 2004; Branco and Häusser, 2010; Stuart and Spruston, 2015), the input–output relationship was investigated with a focus on postsynaptic activity, either by uncaging neurotransmitters or by temporally

controlling electrical stimulation. However, modulations of presynaptic neurotransmitter release have never been examined *in vivo*. This is extremely difficult in the other animal models that have been previously investigated, such as insects and mammals, because (unlike nematodes) they have highly complex neural networks. Focusing on neurotransmitter input and the Ca^{2+} response of postsynaptic neurons, we identified modulation of both input and postsynaptic neuronal activity *in vivo*. In this report, we demonstrate that visualizing synaptic input is a powerful tool for elucidating the input–output relationship *in vivo*.

We showed that synaptic-vesicle release was modulated by odor pre-exposure, and G protein- γ-subunit is necessary for the adaptation. Although we have examined VGLUT-pHluorin or iGluSnFR imaging under AWC-specific RNAi of *gpc-1* conditions, no sensor-expressing strain was obtained. We failed to support our conclusion additionally, but AWC is the only neuron, which has been reported to detect IAA (Bargmann, 2006). Then, the process from the odor detection to the synaptic release from AWC should occurred inside AWC neurons. Furthermore, AWC-specific RNAi abolished early adaptation at behavioral levels (Yamada et al., 2009). From these

studies and our results, it is reasonable to consider that GPC-1 could work in AWC for early adaptation, and modulate the synaptic releasing.

For the modulation of synaptic release, several mechanisms have been reported (Sossin, 2007; Atwood et al., 2014; de Jong and Fioravante, 2014; Friauf et al., 2015; Petzoldt et al., 2016; Bouvier et al., 2018; Nanou and Catterall, 2018). One such mechanisms is G protein-related, and previous research has shown that the γ-subunit regulates the direct fusion of the synaptic vesicle via the soluble N-ethylmaleimide-sensitive factor attachment protein receptor (SNARE) protein (Blackmer, 2001; Blackmer et al., 2005; Gerachshenko et al., 2005; Betke et al., 2012; Atwood et al., 2014). Here, we showed that the G protein γ-subunit, GPC-1, is required to modulate glutamate release (Fig. 5). GPC-1 operates in AWC neurons, and based on its localization, it has been proposed that GPC-1 acts near the synapses (Yamada et al., 2009). Since this mechanism does not include Ca^{2+} response modulation (Blackmer, 2001; Blackmer et al., 2005; Gerachshenko et al., 2005; Betke et al., 2012; Atwood et al., 2014), it may explain the glutamate-release modulation without Ca^{2+} modulation that we observed in the AWC neurons. Another potential mechanism is related to

protein kinase C (PKC). PKC is modulated by decreases in Ca^{2+} levels (Fioravante and Regehr, 2011; Regehr, 2012; de Jong and Fioravante, 2014), so, Ca^{2+} decreasing during 5-min odor pre-exposure in AWC could modulate PKC activity. Moreover, in the sensory neurons of *C. elegans*, PKC regulates synaptic-vesicle release (Ventimiglia and Bargmann, 2017; Hawk et al., 2018), and is included in the synaptic-vesicle release process that its modulated by G protein (Sossin, 2007; Wierda et al., 2007; Kunitomo et al., 2013; Koelle, 2018). Therefore, PKC-dependent modulation is also a possible mechanism.

Acknowledgements

This research was supported by JSPS Grants-in-Aid for JSPS Fellows Grant Number 14J06037. Some plasmids for expression for the indicators were provided by a Grant-in-Aid for Scientific Research on Innovative Areas (Comprehensive Brain Science Network) from the Ministry of Education, Science, Sports and Culture of Japan. We would like to thank Prof. Loren Looger and HHMI Janelia Farm for providing iGluSnFR plasmids. We would like to thank Prof. Cornelia I Bargmann at the Rockefeller University for providing strain and plasmid for VGLUT-pHluorin. N2 and *gpc-1* mutant strains were provided by the CGC, which is funded by NIH Office of Research Infrastructure Programs (P40 OD010440).

Competing interests

The authors declare no competing interests.

Author contributions

K.A. designed the research. K.A. performed all experiments and analysis. K.A. wrote

the first draft of the manuscript. K.A., K.O., K.H., and H.S. edited the manuscript. K.A., K.O., K.H., and H.S. contributed to data interpretation. K.O. and K.H. supervised the research.

Data accessibility

Data used in this paper are available upon request to the corresponding author.

Reference

Ashida K, Hotta K, Oka K (2019) The input-output relationship of AIY interneurons in *Caenorhabditis elegans* in noisy environment. iScience 19:191–203 Available at: https://linkinghub.elsevier.com/retrieve/pii/S2589004219302536.

Atwood BK, Lovinger DM, Mathur BN (2014) Presynaptic long-term depression mediated by Gi/o-coupled receptors. Trends Neurosci 37:663–673 Available at: http://www.ncbi.nlm.nih.gov/pubmed/25160683.

Bargmann C (2006) Chemosensation in *C. elegans*. WormBook Available at: http://www.wormbook.org/chapters/www_chemosensation/chemosensation.html.

Bargmann CI, Hartwieg E, Horvitz HR (1993) Odorant-selective genes and neurons mediate olfaction in *C. elegans*. Cell 74:515–527 Available at: http://linkinghub.elsevier.com/retrieve/pii/009286749380053H.

Betke KM, Wells CA, Hamm HE (2012) GPCR mediated regulation of synaptic transmission. Prog Neurobiol 96:304–321 Available at: https://linkinghub.elsevier.com/retrieve/pii/S030100821200010X.

Blackmer T (2001) G Protein beta gamma subunit-mediated presynaptic inhibition: regulation of exocytotic fusion downstream of Ca^{2+} entry. Science 292:293–297 Available at: http://www.sciencemag.org/cgi/doi/10.1126/science.1058803.

Blackmer T, Larsen EC, Bartleson C, Kowalchyk JA, Yoon E-J, Preininger AM, Alford S, Hamm HE, Martin TFJ (2005) G protein βγ directly regulates SNARE protein fusion machinery for secretory granule exocytosis. Nat Neurosci 8:421–425 Available at: http://www.nature.com/articles/nn1423.

Bouvier G, Larsen RS, Rodríguez-Moreno A, Paulsen O, Sjöström PJ (2018) Towards resolving the presynaptic NMDA receptor debate. Curr Opin Neurobiol 51:1–7 Available at: https://linkinghub.elsevier.com/retrieve/pii/S0959438817302933.

Branco T, Häusser M (2010) The single dendritic branch as a fundamental functional unit in the nervous system. Curr Opin Neurobiol 20:494–502 Available at: https://linkinghub.elsevier.com/retrieve/pii/S0959438810001170.

Brenner S (1974) The genetics of *Caenorhabditis elegans*. Genetics 77:71–94 Available at: http://www.ncbi.nlm.nih.gov/pubmed/4366476.

Chalasani SH, Chronis N, Tsunozaki M, Gray JM, Ramot D, Goodman MB, Bargmann CI (2007) Dissecting a circuit for olfactory behaviour in *Caenorhabditis elegans*. Nature 450:63–70 Available at: http://www.nature.com/articles/nature06292.

Chronis N, Zimmer M, Bargmann CI (2007) Microfluidics for in vivo imaging of neuronal and behavioral activity in *Caenorhabditis elegans*. Nat Methods 4:727–731 Available at: http://www.nature.com/articles/nmeth1075.

Clark DA, Biron D, Sengupta P, Samuel ADT (2006) The AFD sensory neurons encode multiple functions underlying thermotactic behavior in *Caenorhabditis elegans*. J Neurosci 26:7444–7451 Available at: http://www.jneurosci.org/cgi/doi/10.1523/JNEUROSCI.1137-06.2006.

Colbert HA, Bargmann CI (1995) Odorant-specific adaptation pathways generate olfactory plasticity in *C. elegans*. Neuron 14:803–812 Available at: http://linkinghub.elsevier.com/retrieve/pii/0896627395902244.

Cook SJ, Jarrell TA, Brittin CA, Wang Y, Bloniarz AE, Yakovlev MA, Nguyen KCQ, Tang LT-H, Bayer EA, Duerr JS, Bülow HE, Hobert O, Hall DH, Emmons SW (2019) Whole-animal connectomes of both *Caenorhabditis elegans* sexes. Nature 571:63–71 Available at: http://www.nature.com/articles/s41586-019-1352-7.

de Jong APH, Fioravante D (2014) Translating neuronal activity at the synapse: presynaptic calcium sensors in short-term plasticity. Front Cell Neurosci 8 Available at: http://journal.frontiersin.org/article/10.3389/fncel.2014.00356/abstract.

Euler T, Detwiler PB, Denk W (2002) Directionally selective calcium signals in dendrites of starburst amacrine cells. Nature 418:845–852 Available at: http://www.nature.com/articles/nature00931.

Fioravante D, Regehr WG (2011) Short-term forms of presynaptic plasticity. Curr Opin Neurobiol 21:269–274 Available at: https://linkinghub.elsevier.com/retrieve/pii/S0959438811000298.

Friauf E, Fischer AU, Fuhr MF (2015) Synaptic plasticity in the auditory system: a review. Cell Tissue Res 361:177–213 Available at: http://link.springer.com/10.1007/s00441-015-2176-x.

Frick A, Magee J, Johnston D (2004) LTP is accompanied by an enhanced local excitability of pyramidal neuron dendrites. Nat Neurosci 7:126–135 Available at: http://www.nature.com/articles/nn1178.

Gerachshenko T, Blackmer T, Yoon E-J, Bartleson C, Hamm HE, Alford S (2005) Gβγ acts at the C terminus of SNAP-25 to mediate presynaptic inhibition. Nat Neurosci 8:597–605 Available at: http://www.nature.com/articles/nn1439.

Gray JM, Hill JJ, Bargmann CI (2005) A circuit for navigation in *Caenorhabditis elegans*. Proc Natl Acad Sci USA 102:3184–3191 Available at: http://www.pubmedcentral.nih.gov/articlerender.fcgi?artid=546636&tool=pmcentrez&rendertype=abstract.

Hawk JD, Calvo AC, Liu P, Almoril-Porras A, Aljobeh A, Torruella-Suárez ML, Ren I, Cook N, Greenwood J, Luo L, Wang Z-W, Samuel ADT, Colón-Ramos DA (2018) Integration of plasticity mechanisms within a single sensory neuron of *C. elegans* actuates a memory. Neuron 97:356-367.e4 Available at: https://linkinghub.elsevier.com/retrieve/pii/S0896627317311741.

Hirotsu T, Hayashi Y, Iwata R, Kunitomo H, Kage-Nakadai E, Kubo T, Ishihara T, Iino Y (2009) Behavioural assay for olfactory plasticity in *C. elegans*. Protoc Exch Available at: http://www.nature.com/protocolexchange/protocols/582.

Hirotsu T, Iino Y (2005) Neural circuit-dependent odor adaptation in *C. elegans* is regulated by the Ras-MAPK pathway. Genes to Cells 10:517–530 Available at: http://doi.wiley.com/10.1111/j.1365-2443.2005.00856.x.

Horoszok L, Raymond V, Sattelle DB, Wolstenholme AJ (2001) GLC-3: a novel fipronil and BIDN-sensitive, but picrotoxinin-insensitive, L-glutamate-gated chloride channel subunit from *Caenorhabditis elegans*. Br J Pharmacol 132:1247–1254 Available at: http://doi.wiley.com/10.1038/sj.bjp.0703937.

Kerr RA, Schafer WR (2006) Intracellular Ca^{2+} imaging in *C. elegans*. Methods Mol Biol 351:253–264 Available at: http://www.ncbi.nlm.nih.gov/pubmed/16988439.

Koelle MR (2018) Neurotransmitter signaling through heterotrimeric G proteins: insights from studies in *C. elegans*. WormBook:1–52 Available at: http://www.wormbook.org/chapters/www_heterotrimericGproteins.2/neurotransGprotein.html.

Kunitomo H, Sato H, Iwata R, Satoh Y, Ohno H, Yamada K, Iino Y (2013) Concentration memory-dependent synaptic plasticity of a taste circuit regulates salt concentration chemotaxis in *Caenorhabditis elegans*. Nat Commun 4:2210 Available at: http://www.nature.com/articles/ncomms3210.

Marvin JS, Borghuis BG, Tian L, Cichon J, Harnett MT, Akerboom J, Gordus A, Renninger SL, Chen T-W, Bargmann CI, Orger MB, Schreiter ER, Demb JB, Gan W-B, Hires SA, Looger LL (2013) An optimized fluorescent probe for visualizing glutamate neurotransmission. Nat Methods 10:162–170 Available at:

http://www.nature.com/articles/nmeth.2333.

Miesenböck G, De Angelis DA, Rothman JE (1998) Visualizing secretion and synaptic transmission with pH-sensitive green fluorescent proteins. Nature 394:192–195 Available at: http://www.nature.com/doifinder/10.1038/28190.

Nanou E, Catterall WA (2018) Calcium channels, synaptic plasticity, and neuropsychiatric disease. Neuron 98:466–481 Available at: http://linkinghub.elsevier.com/retrieve/pii/S0896627318301946.

Ogawa H, Oka K (2015) Direction-specific adaptation in neuronal and behavioral responses of an insect mechanosensory system. J Neurosci 35:11644–11655 Available at: http://www.jneurosci.org/cgi/doi/10.1523/JNEUROSCI.1378-15.2015.

Ohkura M, Sasaki T, Sadakari J, Gengyo-Ando K, Kagawa-Nagamura Y, Kobayashi C, Ikegaya Y, Nakai J (2012) Genetically encoded green fluorescent Ca^{2+} indicators with improved detectability for neuronal Ca^{2+} Signals. PLoS One 7:e51286 Available at: https://dx.plos.org/10.1371/journal.pone.0051286.

Petzoldt AG, Lützkendorf J, Sigrist SJ (2016) Mechanisms controlling assembly and plasticity of presynaptic active zone scaffolds. Curr Opin Neurobiol 39:69–76 Available at: https://linkinghub.elsevier.com/retrieve/pii/S0959438816300447.

Prešern J, Triblehorn JD, Schul J (2015) Dynamic dendritic compartmentalization underlies stimulus-specific adaptation in an insect neuron. J Neurophysiol 113:3787–3797 Available at: http://www.physiology.org/doi/10.1152/jn.00945.2014.

Regehr WG (2012) Short-term presynaptic plasticity. Cold Spring Harb Perspect Biol 4:a005702–a005702 Available at: http://cshperspectives.cshlp.org/lookup/doi/10.1101/cshperspect.a005702.

Serrano-Saiz E, Poole RJ, Felton T, Zhang F, De La Cruz ED, Hobert O (2013) Modular control of glutamatergic neuronal identity in *C. elegans* by distinct homeodomain proteins. Cell 155:659–673 Available at: http://linkinghub.elsevier.com/retrieve/pii/S0092867413012269.

Shidara H, Hotta K, Oka K (2017) Compartmentalized cGMP responses of olfactory sensory neurons in *Caenorhabditis elegans*. J Neurosci 37:3753–3763 Available at: http://www.jneurosci.org/lookup/doi/10.1523/JNEUROSCI.2628-16.2017.

Shidara H, Kobayashi J, Tanamoto R, Hotta K, Oka K (2013) Odorant-induced

membrane potential depolarization of AIY interneuron in *Caenorhabditis elegans*. Neurosci Lett 541:199–203 Available at: https://linkinghub.elsevier.com/retrieve/pii/S0304394013001262.

Sossin WS (2007) Isoform specificity of protein kinase Cs in synaptic plasticity. Learn Mem 14:236–246 Available at: http://www.learnmem.org/cgi/doi/10.1101/lm.469707.

Stuart GJ, Spruston N (2015) Dendritic integration: 60 years of progress. Nat Neurosci 18:1713–1721 Available at: http://www.nature.com/articles/nn.4157.

Ventimiglia D, Bargmann CI (2017) Diverse modes of synaptic signaling, regulation, and plasticity distinguish two classes of *C. elegans* glutamatergic neurons. Elife 6 Available at: https://elifesciences.org/articles/31234.

Wenick AS, Hobert O (2004) Genomic cis-regulatory architecture and trans-acting regulators of a single interneuron-specific gene battery in *C. elegans*. Dev Cell 6:757–770 Available at: http://linkinghub.elsevier.com/retrieve/pii/S1534580704001650.

White JG, Southgate E, Thomson JN, Brenner S (1986) The structure of the nervous system of the nematode *Caenorhabditis elegans*. Philos Trans R Soc B Biol Sci 314:1–340 Available at: http://rstb.royalsocietypublishing.org/cgi/doi/10.1098/rstb.1986.0056.

Wierda KDB, Toonen RFG, de Wit H, Brussaard AB, Verhage M (2007) Interdependence of PKC-dependent and PKC-independent pathways for presynaptic plasticity. Neuron 54:275–290 Available at: https://linkinghub.elsevier.com/retrieve/pii/S0896627307002504.

Yamada K, Hirotsu T, Matsuki M, Kunitomo H, Iino Y (2009) GPC-1, a G protein-subunit, regulates olfactory adaptation in *Caenorhabditis elegans*. Genetics 181:1347–1357 Available at: http://www.genetics.org/cgi/doi/10.1534/genetics.108.099002.

Yoshida K, Hirotsu T, Tagawa T, Oda S, Wakabayashi T, Iino Y, Ishihara T (2012) Odour concentration-dependent olfactory preference change in *C. elegans*. Nat Commun 3:739 Available at: http://www.nature.com/articles/ncomms1750.

Zhao Y, Araki S, Wu J, Teramoto T, Chang Y-F, Nakano M, Abdelfattah AS, Fujiwara M, Ishihara T, Nagai T, Campbell RE (2011) An expanded palette of genetically encoded Ca^{2+} Indicators. Science 333:1888–1891 Available at:

http://www.sciencemag.org/cgi/doi/10.1126/science.1208592.

Figure legends

Fig. 1 The Ca^{2+} response is not modulated in AWC neurons. (A) Experimental schema. Worms were exposed to S-basal buffer or IAA diluted to a concentration of 10^{-4} in S-basal buffer (see Materials and Methods). (B, C) Ca^{2+} responses with and without odor pre-exposure in the soma (B) and axon (C) in AWC neurons. Red and blue lines indicate the responses with (exposed) and without (control) odor pre-exposure (B, C; left), respectively. The peak Ca^{2+} response intensity following odor removal with (red, exposed) and without (blue, control) odor pre-exposure (B, C; right). Box plots include the median (center line), quartiles (boxes), and range (whiskers). The statistical values are as follows: soma first: $t_{11.45} = -2.67$, $p = 0.021$; soma second: $t_{10.7} = 0.466$, $p = 0.65$; soma decrease: $t_{15.15} = -2.91$, $p = 0.01$; axon first: $t_{8.29} = 1.37$, $p = 0.31$; axon second: $t_{14.134} = 1.53$, $p = 0.15$; axon decrease: $t_{14.6} = 0.423$, $p = 0.68$. Welch's t-test (control: n = 9 and exposed: n = 10). *$p < 0.05$. The shaded regions indicate the standard error of the mean (SEM). Black bars indicate 20 s of IAA stimulation.

Fig. 2 The Ca^{2+} response in AIY interneurons decreases as a result of early adaptation. (A) Experimental schema. Worms were exposed to S-basal buffer or IAA diluted to a concentration of 10^{-4} in S-basal buffer (see Materials and Methods). (B) The AIY Ca^{2+} response with (red) and without (blue) odor pre-exposure, as assessed using G-CaMP6 and dimer2 imaging (left). The blue box plot (right) shows the peak intensity for the no odor pre-exposure condition (control), and the red box plot indicates the peak intensity for the odor pre-exposure condition (exposed). Box plots include the median (center line), quartiles (boxes), and range (whiskers). The statistical metrics are followings: $t_{45.2} = 2.21$, $p = 0.032$, Welch's t-test (without pre-exposure: n =26 and with pre-exposure: n = 26). *$p < 0.05$. The black bar indicates 40 s of IAA stimulation. Shaded regions indicate the SEM.

Fig. 3 Glutamate inputs to AIY neurons are modulated by early adaptation. (A) Experimental schema. Worms were exposed to S-basal buffer or IAA diluted to a concentration of 10^{-4} in S-basal buffer (see Materials and Methods). (B) Glutamate inputs to AIY neurons with and without odor pre-exposure. The red and blue lines indicate the response with (exposed) and without (control) odor pre-exposure, respectively. The black bars indicate 20 s of IAA stimulation. The shaded regions indicate the SEM. (C) Changes in glutamate input to AIY neurons as a result of odor stimulation. Glutamate input changes in response to odor in AIY with and without odor pre-exposure. The box plots indicate increases following first odor removal (first: 20–40 s, second: 140–160 s, see also Materials and Methods) and decreases in response to the second odor addition (decrease: 120–140 s, see also Materials and Methods). The red and blue graphs are the results with and without odor pre-exposure, respectively. Box plots include the median (center line), quartiles (boxes), and range (whiskers). The statistical metrics are followings: the first: $t_{11.0} = 4.56$, $p = 0.00051$; the second: $t_{14.4} = 2.81$, $p = 0.014$; the decrease: $t_{16.7} = 3.16$, $p = 0.0058$, Welch's t-test (control: $n = 9$ and exposed: $n = 11$). (D) Averaged glutamate input intensity before and during odor

application. Intensities were normalized at 80 s. The blue and red plots indicate the no odor (control) and odor pre-exposure (exposed) results, respectively. The plots with lines indicate the results in the same animals. The boxes indicate the average values. The statistical metrics are as follows: control data comparison between pre- and during odor stimulation: $t_8 = 4.60$, $p = 0.0018$; exposed data comparison between pre- and during odor stimulation: $t_{10} = -0.662$, $p = 0.61$, paired sample t-test (control: n = 9 and exposed: n = 11). *p < 0.05; **p < 0.01; N. S., not significant (p > 0.05).

Fig. 4 Modulation of AWC synaptic-vesicle release. (A) Experimental schema: to avoid the severe effects of fluorescent bleaching, only responses to the second stimulation were recorded. (B) Synaptic release in the AWC neurons with and without odor pre-exposure. The red and blue line indicate the responses with (exposed) and without odor pre-exposure (control), respectively. The black bar indicates 20 s of IAA stimulation. Shaded regions indicate the SEM. (C) Synaptic-release changes in response to odor with and without odor pre-exposure. The graphs show the decrease in response to odor addition (left) and increase following odor removal (right). The red and blue box plots indicate the results for odor (exposed) and no odor pre-exposure (control), respectively. Box plots include the median (center line), quartiles (boxes), and range (whiskers). The statistical metrics are as follows: decrease: $t_{11.9} = -2.24$, $p = 0.045$; increase: $t_{15.0} = 2.17$, $p = 0.047$, Welch's t-test (control: $n = 9$; exposed: $n = 8$). *$p < 0.05$; **$p < 0.01$.

Fig. 5 *gpc-1* mutants are defective under glutamate modulation. (A) Chemotaxis of wild-type and *gpc-1* mutant animals. Chemotaxis assays were performed with no pre-exposure (control), with IAA pre-exposure (exposed) and with S-basal buffer pre-exposure (mock). Box plots include the median (center line), quartiles (boxes), and range (whiskers). The statistical metrics are as follows: wild-type exposed: t = -4.38, p = 0.00022; wild-type mock: t = -0.661, p = 0.75; *gpc-1* exposed: *t* = -1.75, p = 0.17; *gpc-1* mock: t = -1.38, p = 0.31, Dunnett's test for comparing the control with the other conditions (wild-type control: n = 18; wild-type exposed: n = 14; wild-type mock: n = 5; *gpc-1* control: n = 7; *gpc-1* exposed: n = 8; *gpc-1* mock: n = 5). ***p < 0.001. (B) Glutamate inputs to AIY interneurons with and without odor pre-exposure in *gpc-1* mutants. The red and blue lines are the response with (exposed) and without odor pre-exposure (control), respectively. The black bars indicate 20 s of IAA stimulation. The shaded regions indicate the SEM. (C) Peak and decreased glutamate intensities for glutamate input with and without odor pre-exposure in *gpc-1* mutants. The box plots indicate increases in response to odor removal (first and second) and decreases following the second odor addition (decrease). The red blue graphs are the results with

and without odor pre-exposure, respectively. Box plots include the median (center line), quartiles (boxes), and range (whiskers). The statistical metrics are as follows: first exposure: $t_{10.7} = -0.315$, $p = 0.76$; second exposure: $t_{10.4} = -0.146$, $p = 0.89$; decrease: $t_{10.9} = -0.357$, $p = 0.73$, Welch's t-test (control: n =6; exposed: n = 7). N. S., not significant ($p > 0.05$). (D) Averaged glutamate input intensities before and during odor exposure. We normalized intensities at 80 s. The red and blue plots indicate the results with (exposed) and without odor pre-exposure (control), respectively. The plots with lines indicate the results in the same animals. The bars indicate the average values. The statistical metrics are as follows: control data comparison between pre- and during odor stimulation: $t_5 = 7.13$, $p = 0.00084$; exposed data comparison between pre- and during odor stimulation: $t_6 = 2.84$, $p = 0.030$, paired sample t-test (control: n =6; exposed: n = 7). *$p < 0.05$; ***$p < 0.001$; N. S., not significant ($p > 0.05$).

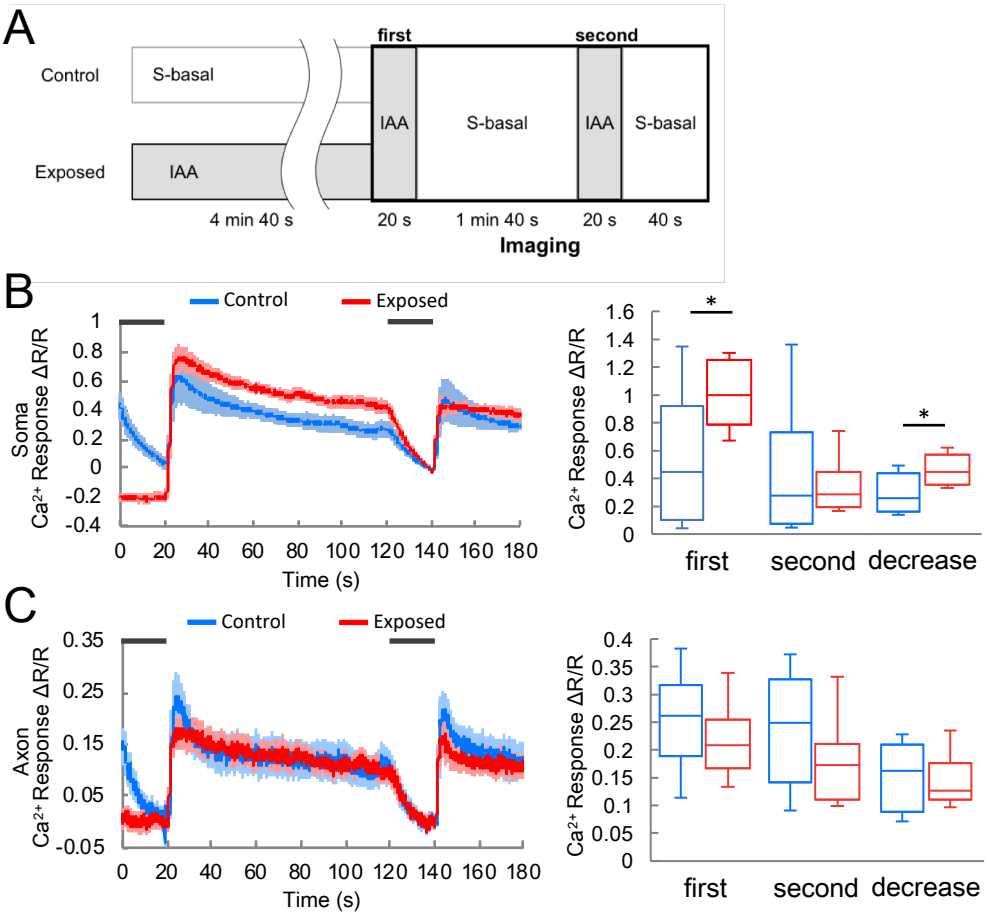
A
first
second
Control
S-basal
IAA
S-basal
IAA
S-basal
Exposed
IAA
4 min 40 s
20 s
1 min 40 s
20 s
40 s
Imaging
B
Control
Exposed
Soma
Ca2+ Response ΔR/R
Time (s)
first
second
decrease
C
Control
Exposed
Axon
Ca2+ Response ΔR/R
Time (s)
first
second
decrease

Figure 1

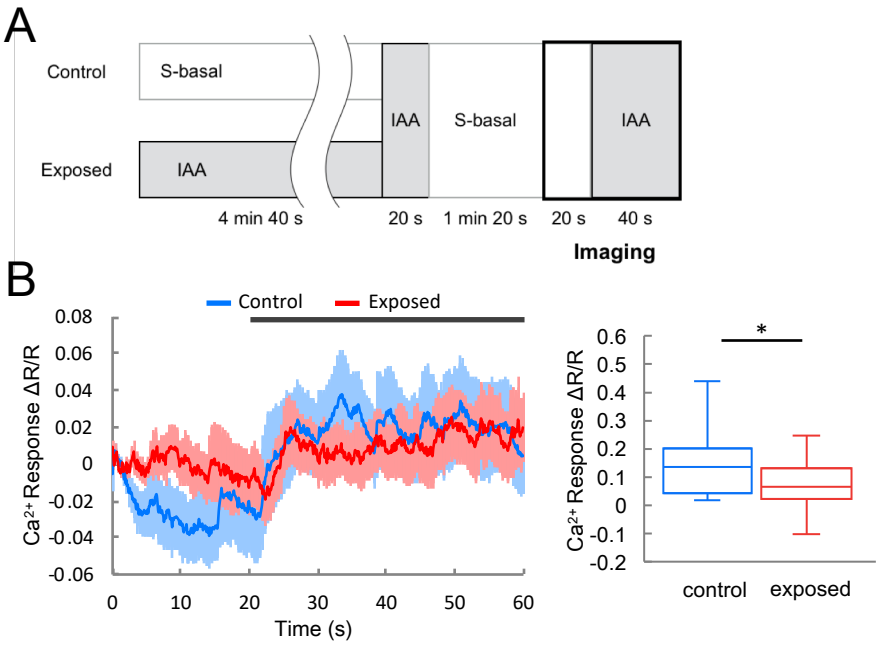
A
Control
S-basal
IAA
S-basal
IAA
Exposed
IAA
4 min 40 s
20 s
1 min 20 s
20 s
40 s
Imaging
B
Control
Exposed
0.08
0.06
0.04
0.02
0
-0.02
-0.04
-0.06
Ca2+ Response ΔR/R
0
10
20
30
40
50
60
Time (s)
*
0.6
0.5
0.4
0.3
0.2
0.1
0
-0.1
-0.2
Ca2+ Response ΔR/R
control
exposed

Figure 2

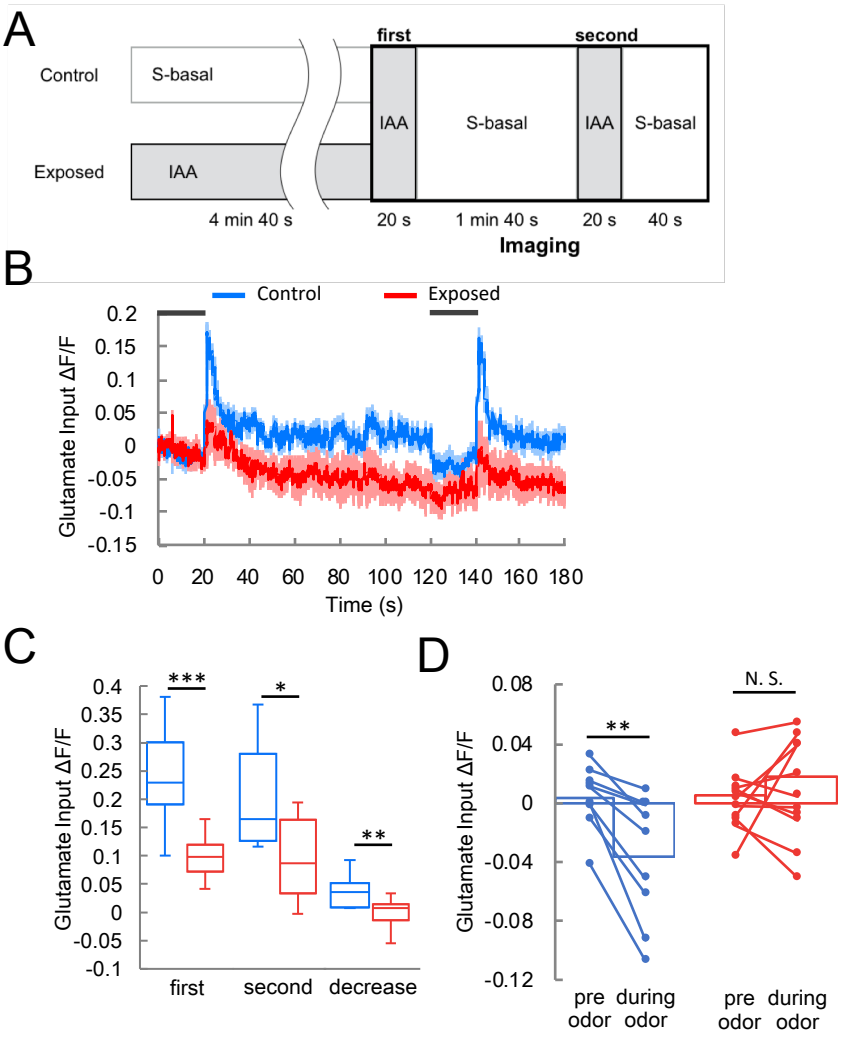
A
first
second
Control
S-basal
IAA
S-basal
IAA
S-basal
Exposed
IAA
4 min 40 s
20 s
1 min 40 s
20 s
40 s
Imaging
B
Control
Exposed
Glutamate Input ΔF/F
0.2
0.15
0.1
0.05
0
-0.05
-0.1
-0.15
0
20
40
60
80
100
120
140
160
180
Time (s)
C
Glutamate Input ΔF/F
0.4
0.35
0.3
0.25
0.2
0.15
0.1
0.05
0
-0.05
-0.1
***
*
**
first
second
decrease
D
Glutamate Input ΔF/F
0.08
0.04
0
-0.04
-0.08
-0.12
**
N. S.
pre odor
during odor
pre odor
during odor

Figure 3

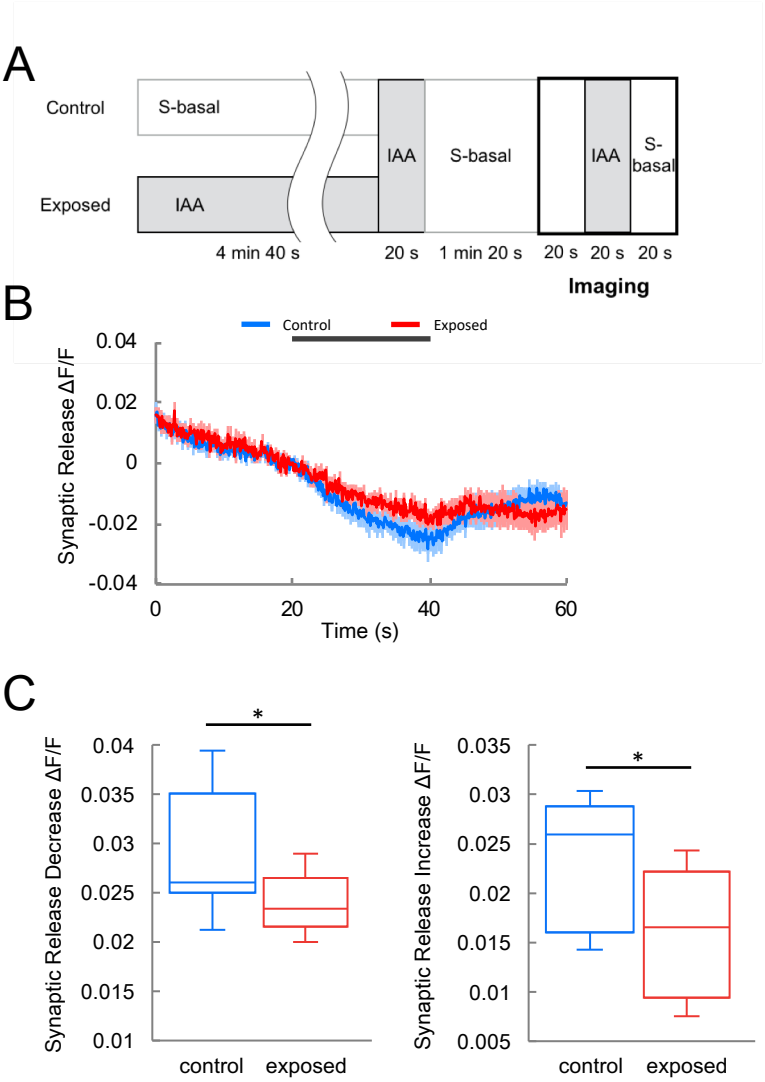
A
Control
S-basal
Exposed
IAA
IAA
S-basal
IAA
S-basal
4 min 40 s
20 s
1 min 20 s
20 s
20 s
20 s
Imaging
B
Control
Exposed
Synaptic Release ΔF/F
0.04
0.02
0
-0.02
-0.04
0
20
40
60
Time (s)
C
Synaptic Release Decrease ΔF/F
0.04
0.035
0.03
0.025
0.02
0.015
0.01
*
control
exposed
Synaptic Release Increase ΔF/F
0.035
0.03
0.025
0.02
0.015
0.01
0.005
*
control
exposed

Figure 4

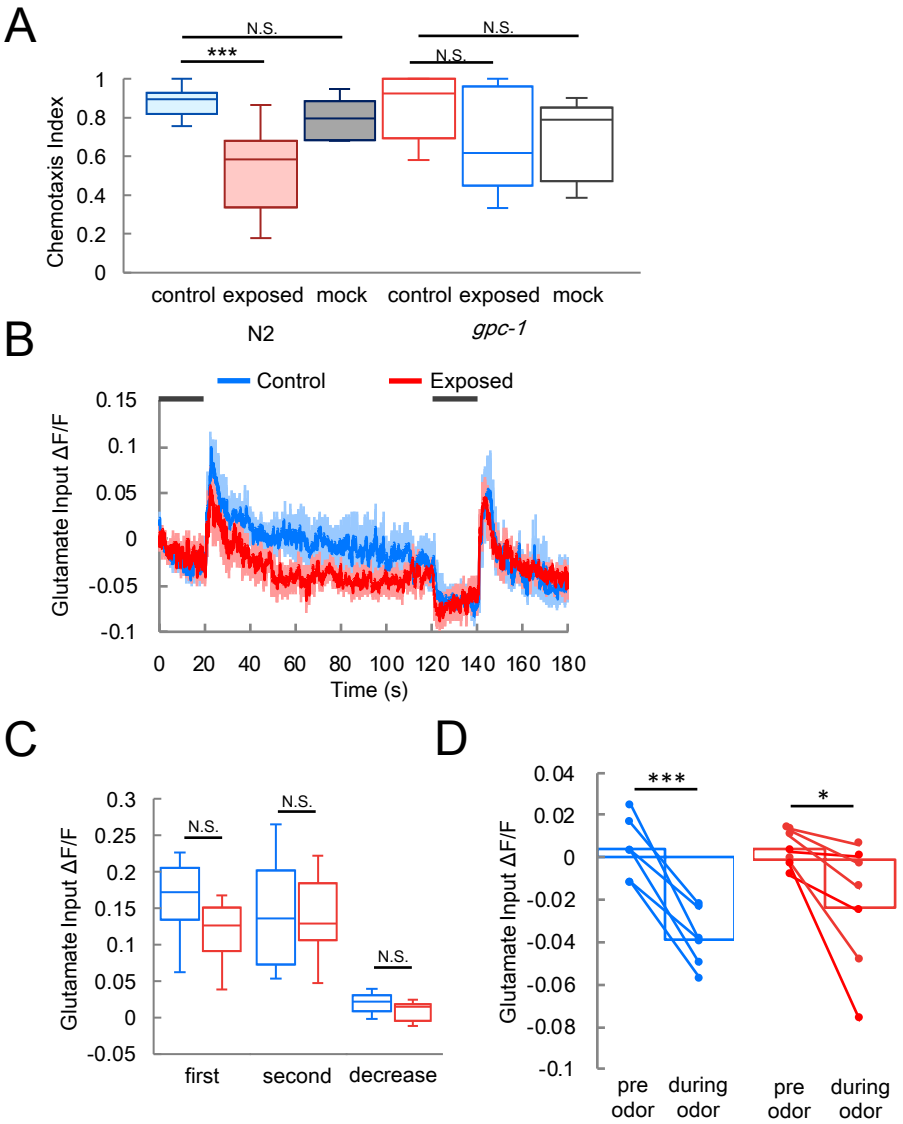
A
N.S.
***
N.S.
N.S.
Chemotaxis Index
1
0.8
0.6
0.4
0.2
0
control exposed mock control exposed mock
N2
gpc-1
B
Control
Exposed
Glutamate Input ΔF/F
0.15
0.1
0.05
0
-0.05
-0.1
0 20 40 60 80 100 120 140 160 180
Time (s)
C
Glutamate Input ΔF/F
0.3
0.25
0.2
0.15
0.1
0.05
0
-0.05
N.S.
N.S.
N.S.
first
second
decrease
D
Glutamate Input ΔF/F
0.04
0.02
0
-0.02
-0.04
-0.06
-0.08
-0.1
***
*
pre odor
during odor
pre odor
during odor

Figure 5